Nano Communication Networks 1 (2010) 63–75

Contents lists available at ScienceDirect

Nano Communication Networks

journal homepage: www.elsevier.com/locate/nanocomnet

A nanoradio architecture for interacting nanonetworking tasks

C. Emre Koksal, Eylem Ekici *

Department of Electrical and Computer Engineering, The Ohio State University, 43210 Columbus, OH, United States

ARTICLE INFO

Article history:
Received 3 February 2010
Accepted 8 March 2010
Available online 2 May 2010

Keywords:
Nanocommunication
Nanoscale networks
Carbon nanotube transceivers
Detection theory

ABSTRACT

Nanotechnology has the potential to have a significant impact on a number of application areas. The possibility of building components at the nanoscale revolutionized the way we think about systems by enabling myriad possibilities, that were simply impossible otherwise. At the same time, countless challenges were raised in system design. One such challenge is to build components that act together to handle complex tasks that require physically separate components to work in unison. To achieve coordination, these components have to be capable of communicating reliably, either with a central controller or amongst themselves. In this research, we propose to build analytical foundations to analyze and design nanonetworks, consisting of individual stations communicating over a wireless medium using nanotransceivers with nanotube antennas. We give a simple nanoreceiver design and analyze its basic limitations. Based on the insights drawn, we propose a communication-theoretic framework to design reliable and robust nanoreceivers. With the basic limitations of the nanocommunications via nanoantennas in mind, it is possible to develop mathematical tools to help construct nanonetworks that execute basic sequential tasks in a reliable manner with minimal amount of communication and computation required. In this paper, we present a communication-theoretic analysis of networks of nanoscale nodes equipped with carbon nanotube-based receivers and transmitters. Our objective is to analyze the performance characteristics of nanoscale nodes and expose their fundamental capabilities and limitations. The presented analysis is intended to serve as the basis of nanonetwork design enabling various applications.

1. Introduction and motivation

Nanotechnology has the potential to have a significant impact on a number of application areas including health care [7,14,15], bio-hybrid implants [11,16], food and water quality control [3], defense systems against biological and chemical attacks [33], air pollution control [20], and biodegradation [1]. The possibility of building components at the nanoscale revolutionized the way we think about systems by enabling myriad possibilities, that were simply impossible otherwise. At the same time, countless challenges were raised in system design. One such challenge is to build components that act together to handle complex tasks that require physically separate components to work in unison. To achieve coordination, these components have to be capable of **communicating reliably**, either with a central controller or amongst themselves. In this research, we propose to build analytical foundations to analyze and design **nanonetworks**, consisting of individual stations communicating over a wireless medium using **nanotransceivers** with **nanotube antennas**. We give a simple nanoreceiver design and analyze its basic limitations. Based on the insights drawn, we propose a **communication-theoretic framework** to design **reliable and robust nanoreceivers**. With the basic limitations of the *nanocommunications* via nanoantennas in mind, it is possible to develop mathematical tools to help construct nanonetworks that execute

* Corresponding author. Tel.: +1 614 292 0495; fax: +1 614 292 7596.
E-mail addresses: koksal@ece.osu.edu (C. Emre Koksal), ekici@ece.osu.edu (E. Ekici).

1878-7789/$ – see front matter © 2010 Elsevier Ltd. All rights reserved.
doi:10.1016/j.nancom.2010.03.001

basic sequential tasks in a reliable manner with minimal amount of communication and computation required.

The physical operation of a nanotube antenna is significantly different from that of a classical antenna for wireless communication. The nanotube absorbs electromagnetic waves and converts them to mechanical vibrations. Since the nanotube is charged, these vibrations cause changes in the electric field at the cathode right across the nanotube and the induced current is processed to recover the incident signal. Since the mechanism of the nanotube antenna is electromechanical, the nanoreceiver has to overcome the **acoustic noise**, which is effective directly on the nanotube, as well as the **thermal noise**, effective at the rear end of the antenna. The unconventional physics of nanotube antennas and the various noise sources one has to consider makes the design of nanoreceivers and the analysis of their performance a highly challenging task.

Another challenge in the design of nanoreceivers stems from the limitations of components at the nanoscale. Nanoelectronic manufacturing is at its infancy stage, and a nanoreceiver cannot involve hardware components apart from some very basic ones. For example, a detection scheme cannot involve any computations beyond the most trivial ones, such as a mere comparison. Consequently, the associated team tasks have to be simple to implement.

The analysis presented in this paper lays the groundwork to design nanonetworks, consisting of nodes individually responsible for a certain number of basic tasks. To achieve these tasks, the nodes must be **activated**, either externally by a centralized controller, or internally in a sequential manner as the activation signal propagates in the network in a **multihop** fashion. The activation signal is an electromagnetic wave of a certain duration, tuned according to the resonance frequency of the nanotube antennas of the nodes to be activated. Note that this construct can be useful in a number of applications. For instance, in a **drug delivery system**, once activated, each node can be responsible for releasing a certain drug in some desired order. The node can send the activation signal for the desired *next hop* in the sequence, once releasing its chemicals after being activated. Coupled with sensing devices, automated dosage control can be integrated into the drug delivery system, as well. Also, one can consider a **nano-RFID** application, in which each node can be viewed as an RFID, emitting a certain signal once active. Furthermore, multihop activation of nodes can mimic the effect of the nervous system through the propagation of activation signals in a bio-hybrid implant such as **artificial muscle tissues** to coordinate the activation of different parts of the tissue.

In designing such systems, **reliability** is the major issue and one has to be careful in the possibility of the following events.

(1) A node can go active, even in the absence of an activation signal. This can be catastrophic in a number of applications including drug delivery. One has to make sure that the *probability* of a **false activation** event is very low even in the time scale of months/years of continual operation.

(2) A node can remain inactive, even after the activation signal is sent to it. This event can be highly undesirable, especially in applications that require a timely response. One has to guarantee that the *probability* of an **unsuccessful activation** event is below a certain threshold each time the activation signal is sent to a node. There is clearly a tradeoff between the probability of false activation and the probability of unsuccessful activation.

(3) There are a number of imperfections associated with the system components. Examples of such imperfections include the **frequency and timing mismatch** between the activator and the receiver, and model imperfections and parameter uncertainties at the nanoscale. Nanoreceiver design should be robust with respect to such imperfections.

(4) If the activation signals are chosen to be "close" to each other, the probabilities of unsuccessful and false activation events increase, due to **crosstalk** among different nodes. This imposes a fundamental limit on the number of activation signals, and hence the tasks the network can handle, for a given limited amount of usable bandwidth. The network must be designed with this limitation taken into account.

(5) The **delay** in the execution of certain tasks can be too high to be tolerable. This can be caused by a high activation time of individual events in a sequence or through failures in sensing physical phenomena. Designed systems must ensure not only the eventual completion of a sequence of tasks, but also their successful completion within tolerable delay limits.

In this paper, we present a communication-theoretic analysis of networks of nanoscale nodes equipped with carbon nanotube-based receivers and transmitters. Our objective is to analyze the performance characteristics of nanoscale nodes and expose their fundamental capabilities and limitations. The presented analysis is intended to serve as the basis of nanonetwork design enabling various applications.

The remainder of the paper is organized as follows. In Section 2, a brief summary of related work in the literature is presented. The system architecture and the network model are presented in Section 3. Analysis of single-node activation is discussed in Section 4, followed by multi-node activation analysis in Section 5. The paper is concluded in Section 7.

2. Related work

Recent advances in nanotechnology have resulted in the development of nanoscale machinery such as molecular elevators [4], nanoswitches [8], chemical sensors [27,25], nanoactuators [12,24], and carbon nanotube receivers [22] and transmitters [35]. The main mechanisms to manufacture nanomachinery involve three approaches [1]. The top-down approach aims to manufacture nanomachinery through the miniaturization of microscale devices to the nanoscale. Electron beam lithography [21,34] and microcontact printing [26] are two main tools used in this approach. Great strides are being made in the manufacturing of individual components [6], and simple structures such as nanogears are fabricated via this approach [36]. The bottom-up approach aims to form nanomachines using molecules as the basic building blocks. Also called

molecular manufacturing [11], this approach has theoretically been shown to be very useful to fabricate a variety of components including molecular pumps [29]. Finally, the third approach to nanomachinery manufacturing is the bio-hybrid approach, which models the nanomachinery after biological structures such as cells. Using bacteria to propel microscale objects follows the bio-hybrid approach to nanoscale manufacturing [5].

These nanomachines cannot accomplish complex tasks outlined in Section 1 by themselves and should be combined into **nanonodes**. Complex tasks and applications require interaction among nanonodes, exchange of information, and execution of tasks conditioned on environmental inputs. Communication between nanonodes can occur via nanomechanical interactions, diffusion and exchange of chemicals, through pressure waves, or electromagnetic signals [17]. Among these options, molecular diffusion techniques [30,28] and nanomechanical interactions [19] have been envisioned as means of long-range and short/medium-range communication for nanonetworks, respectively. Long considered as infeasible due to projected size and complexity resulting from miniaturization-based transceiver design [17], RF-based communication has captured the limelight of nanocommunication research through the development of nanoscale receivers [22] and transmitters [35]. Tests performed on prototypes of these devices have proved not only the feasibility of nanoscale transceivers, but also manufacturing possibilities using today's technology. Therefore, carbon nanotube-based transmitters and receivers are considered as most promising enablers of RF-based communication at the nanoscale. Along these lines, a carbon nanotube-based sensor network architecture has also been introduced in the literature [2]. However, the fundamental properties of communication via carbon nanotube-based transmitters and receivers have not been investigated in detail, which is the focus of this paper.

In the literature, there are a limited number of network architecture proposals using nanomachinery and nanonodes. In [1], high-level network architectures involving communication via molecular motors, diffusion-based calcium signaling, and pheromones have been introduced and discussed. A bio-hybrid architecture involving bacteria and nanomotors has been introduced in [19]. The common thread in these proposals is the simplicity in interaction and specificity of tasks to be performed, which parallels the design principles of our vision for nanonetworks. As the first step of system design, we provide a rigorous characterization of RF-based communication in nanonetworks.

3. System architecture and modeling

3.1. Physics of nanotube antennas

A nanotube antenna is composed of a carbon nanotube attached to a cathode. The carbon nanotube vibrates according to the incident electric field's intensity and frequency, which causes variations in the electron emission from the tip of the carbon nanotube. The induced current formed at the cathode is detected at the output of the rear end of the nanotube antenna, which we will refer to as the *nanoantenna*. In the rest of this section, we briefly describe the physical behavior of a nanoantenna (for a detailed description, see [22]) and our abstract model for a nanoantenna as well as for our *nanoreceiver* will be given in the following section.

In Fig. 1(a), the schematic of the nanoantenna receiver is shown. The resonance frequency f_0 of the carbon nanotube is given as $f_0 = \frac{0.56}{L^2}\sqrt{\frac{YI}{\rho A}}$, where L is the length of the nanotube, Y is the Young's modulus, I is the areal moment of inertia with $I = (\pi/4)(r_o^4 - r_i^4)$ for a cylinder with outer and inner radii r_o and r_i, ρ is the density, and A is the cross-sectional area. Typical values for these parameters, $L \approx 250$ nm and $r \approx 5$ nm, result in a resonance frequency range of 10–100 MHz [22]. The amplitude of the vibrations $|Y_o|$ is given by $|Y_o| = \frac{qE_{\text{rad}}/m_{\text{eff}}}{4\pi^2\sqrt{(f^2-f_0^2)^2+(ff_0/Q)^2}}$, where q is the charge of the tip of the nanotube with $q \approx 3 \times 10^{-17}$ C, E_{rad} is the amplitude of the electric field of the incoming transmission, $m_{\text{eff}} = 0.24m$ is the effective mass of the nanotube with m being the actual weight, f_0 is the resonance frequency, f is the frequency of the incoming transmission, and Q is the quality factor, with typical values around 500.

The field emission current from the tip of the carbon nanotube is described as $I_r = c_1 A(\gamma E_{\text{ext}})^2 e^{-\frac{c_2}{\gamma E_{\text{ext}}}}$, where A is the area from which the nanotube emits electrons, E_{ext} is the external applied electric field, c_1 and c_2 are constants specific to nanotube behavior, and γ is the local field enhancement factor. The field enhancement factor can be approximated as $\gamma = 3.5 + \frac{h}{r}$, where h is the height of the tip of the nanotube above the cathode (see Fig. 1(a)) and r is the radius of the nanotube. As the nanotube vibrates, the height of its tip oscillates resulting in a time-varying field enhancement factor $\gamma(t) = \gamma_0 + \Delta\gamma(t)$. Expanding to second order in powers of $\Delta\gamma(t)/\gamma_0$ and filtering out the zeroth and first powers of $\Delta\gamma(t)/\gamma_0$, which correspond to DC and RF terms, yields $\Delta I_r(t) = I_0(1 + \alpha + \alpha^2/2)(\Delta\gamma(t)/\gamma_0)^2$; $\alpha = \frac{c_2}{\gamma_0 E_{\text{ext}}}$.

The above-described setup accounts for the reception of an RF signal using a carbon nanotube. Similarly, in [35], the basic setup for a nanomechanical transmitter is depicted. The main idea is to have the nanotube carry a charge at its tip and have it mechanically oscillate, effectively producing electromagnetic waves. To this end, the property of the nanotube that mechanical self-oscillations can be induced in a single-clamped nanoscale resonator by applying only a DC voltage is leveraged. Self-oscillations are dependent on field emission from the nanotube to a cathode. This concept can be applied to the nanotube transmitter by adjusting V_{bias}, in Fig. 1(b), to a DC voltage that will cause both field emission and self-oscillations in the nanotube. The nanotube will oscillate at the mechanical resonance frequency. By changing the tension on the nanotube with a voltage on the V_{tension} electrode in Fig. 1(b), the nanotube would bend and therefore change the resonant frequency. The information signal could be applied to this electrode to modulate the frequency of the self-oscillations.

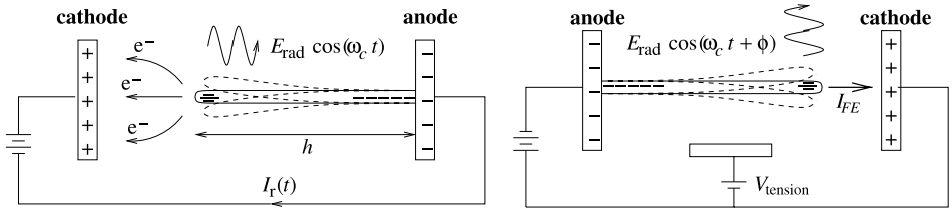

(a) Nanotube radio receiver. (b) Nanotube radio transmitter.

Fig. 1. (a) Nanotube radio receiver. Incident electromagnetic waves cause oscillations of the tip of the nanotube, changing the electron emission rate [22]. (b) Nanotube radio transmitter. Field emission from the tip of the nanotube can induce self-oscillations in the nanotube. In combination with the excess charge in the tip of the nanotube, these mechanical oscillations effectively transmit a radio signal [35].

3.2. Nanoreceiver model

The abstract model for our nanoreceiver based on the physical properties of the described nanoantenna is given in Fig. 2. The basic components of the *front end* include the nanoantenna and the square-law detector. Here, $h_r(t)$ is the impulse response of the linear filter that captures the input–output behavior of the nanoantenna, where the input $Y_i(t)$ is the incoming electromagnetic field and the output $Y_o(t)$ is the amplitude of the associated vibrations. Based on the physical model given in the previous section, the frequency response of the nanoantenna can be found to be

$$H_r(f) = \frac{|Y_o(f)|}{E_{\text{rad}}(f)} = \frac{q/m_{\text{eff}}}{4\pi^2\sqrt{(f^2-f_0^2)^2+(ff_0/Q)^2}}. \quad (1)$$

Since the antenna response is symmetric with respect to the resonance frequency f_0, the 3 dB bandwidth, B, of $H_r(f)$ can be found by solving $H_r(f_0)/\sqrt{2} = H_r(f_0+B)$. With the assumption that $f_0 \gg B$, one can find $B \approx \frac{f_0}{2Q}$. Note that the assumption is highly accurate for the typical values of Q (i.e., between 500–1000). We have a square-law device, since the observed current, $I_r(t)$, is proportional to the square[1] of the amplitude of the vibrations of the nanotube.

We assume that the signal is corrupted by additive white Gaussian noise (AWGN) at two levels: the **acoustic noise**, $W_a(t)$, is the mechanical component that affects the amplitude of the vibrations $Y_o(t)$, whereas the **thermal noise**, $W_T(t)$, is added to the detected current. We denote the two-sided power spectral densities of the acoustic noise and the thermal noise with $N_a/2$ and $N_T/2$, respectively.

For a nanoreceiver to be feasible, low complexity is one of the main constraints. At the nanoscale, even slightly complex components become infeasible. Hence, to achieve node activation, we use a simple energy detector, as shown in Fig. 2. Since the signal $I_r(t)$ is the current at the output of the front end of the receiver, the integrator can be realized by a mere *capacitor*. The integrator is followed by the sampler, sampling the output of the integrator once every T seconds, which we refer to as the **activation period**. We assume that the activation period is much longer than the reciprocal of the 3 dB bandwidth of the antenna response. Hence, we have

$$\frac{1}{T} \ll B \ll f_0. \quad (2)$$

Finally, each sample $Y_s[k]$ is compared with a pair of predetermined thresholds τ_1 and τ_2 (as will be explained in the next section) and the node becomes active depending on these comparisons.

The combination of the square-law device and the integrator acts as a *demodulator* for the waveform $Y_o(t)$. However, note that $Y_o(t)$ also includes the noise component $W_a(t)$, filtered by the antenna response $h_r(t)$. Since we do not have any front-end filter to remove the out-of-band noise components, the performance of the system degrades. This is the price paid to avoid realizing the filter. Notice that, in our energy detector, the only components we used are a capacitor, a sampler and a series of comparators. To activate multiple events at a node, we do not rule out the possibility that a node has **multiple energy detectors**, with multiple nanoantennas of different sizes (and hence different resonance frequencies). This will enable us to activate multiple functions in the same node, without a need for post-processing of the received signal.

3.3. Network model

The network model is based on a low-complexity node architecture and their predefined interactions. The basic structure of a nanonode under consideration consists of power, sensing, actuation, and transceiver units. Although these components are also found in traditional wireless sensor nodes, our proposed architecture is significantly different from that of sensor nodes since a major component, i.e., **processor**, is not present. The reason for this exclusion is that a nanoscale processor with significant computational power is not likely to materialize in the near future. We acknowledge recent efforts and research attempts in realizing processor components at the nanoscale. As an example, nanoscale circuits and components have been proposed in recent years [8,10,18,9]. However, a computational component as we understand today requires significant research and development efforts. On the other hand, research on other components of the node architecture, i.e., energy storage [23], chemical sensors [27,25], molecular-level actuators [12,24] and nanotransceivers [22,35] as well as simple methods to connect

[1] Note that the detected current is proportional to the square of $\Delta\gamma(t)$, which in turn is proportional to the amplitude $|Y_o(t)|$.

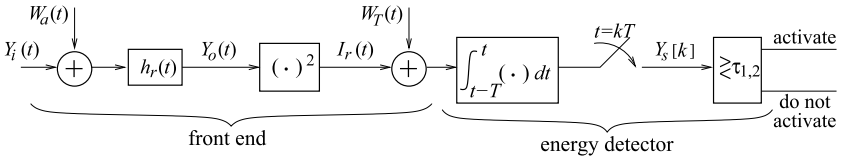

Fig. 2. System model of our nanoreceiver.

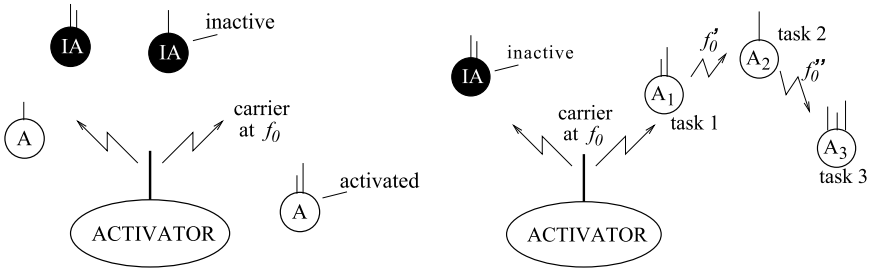

(a) Nodes activated centrally.

(b) Nodes activated centrally and by other nodes for sequential tasks.

Fig. 3. Various nanonetwork architectures for activation of sequential tasks. Multiple antennas enable multiple potential tasks activated for a certain node.

them into systems have matured far more significantly [13]. Each node is assumed to be capable of *sensing* (with a possible binary outcome), *receiving* electromagnetic signals (to activate actions in a nanonode), to possibly *relay* another activation signal, and to act based on the RF-based activation and local stimuli.

Our hypothesis is that one can achieve significant advancements in development of nanoscale machinery even ***without using any significant processing power***.[2] The logical operations to combine received "activation" signals and locally sensed information can be managed through physical pathways that control the actuators and the transmitter blocks. We consider two main architectures of nanonetworks. The first one is the **centralized (cellular) architecture**, where an external activation signal is transmitted to a set of nanonodes as illustrated in Fig. 3(a). Nodes are activated upon reception of the RF signal and they do not directly interact among themselves. Hence, the control of the system is given to the centralized external controller that emits the activation signals. These signals can be transmitted to sequentially activate nanonodes one by one or in groups. The selection of the activation sets is determined by the resonance frequency of the antennas, and consequently, the transmission frequencies. The second architecture is a **multi-hop architecture**, where nodes are not only activated from an external source but can also activate each other as shown in Fig. 3(b). A multi-hop architecture is crucial to accomplish non-trivial sequences of tasks. Combined with the local sensing and actuation capabilities, a network of nodes can be designed to perform tasks in an event-driven manner, accounting for local conditions as well as activation signals external and internal to the nanonetwork. Furthermore, the interactions between nodes can be designed to implement condition-based branching and loops to achieve target stimulus levels without the involvement of an outside controller in the loop.

[2] If and when more sophisticated processing capabilities are available, the effectiveness of such systems would improve, without diminishing the importance of the presented analysis.

4. Single-node activation

In this section, we present a communication theoretic analysis of our receiver, given in Fig. 2. We will consider a single link and provide fundamental limitations involved in node activation. In particular, we will analyze the necessary signal duration T to meet a desired **probability of successful activation**. This gives us an idea of how much energy is required to achieve a certain task. We use this analysis as an initial point for further system design, including the tradeoffs involved in the number of tasks achievable in a given nanonetwork, which we consider in the next section.

To activate a node, we assume that the activator uses pure sinusoids of duration T. Consequently, at the input of the receiver, we have $Y_i(t) = a\cos(2\pi f_0 t + \phi)$, where ϕ is the random phase. The most energy-efficient way of activating a node is to choose the frequency of the sinusoid, identical to the resonance frequency f_0 of the nanoantenna. The signal at the output of the antenna is thus

$$Y_o(t) = \begin{cases} a\cos(2\pi f_0 t + \phi)|H_r(f_o)| + \tilde{W}_a(t), \\ \quad \text{activation attempt} \\ \tilde{W}_a(t), \quad \text{otherwise}, \end{cases} \tag{3}$$

where $H_r(f)$ is the frequency response of the nanoantenna and the acoustic white Gaussian noise, filtered by the antenna response, is denoted by $\tilde{W}_a(t)$, which is also a Gaussian process. Hence, the pre-thermal noise portion of the current at the output of the front-end of the receiver can be written as

$$I_r(t) = \begin{cases} a^2|H_r(f_0)|^2\cos^2(2\pi f_0 t + \phi) + 2a|H_r(f_0)| \\ \quad \times \cos(2\pi f_0 t + \phi)\tilde{W}_a(t) + \tilde{W}_a^2(t), \\ \quad \text{activation attempt} \\ \tilde{W}_a^2(t), \quad \text{otherwise}. \end{cases} \tag{4}$$

The energy detector integrates $I_r(t)+W_T(t)$ over the past T seconds and a sampler samples the output of the integrator every T seconds. We initially disregard the issues of timing and frequency mismatch between the activator and the nanoreceiver in the following analysis. We will analyze the impacts of these imperfections later on.

One can realize that there are three components of $I_r(t)$ under the activation attempt, as given in Eq. (4). The first one is the *signal component*, the second one is the *signal–noise cross-component*, which is a Gaussian process, and the last one is the *noise–noise cross-component*, which has Chi-squared samples. Next we analyze the contribution of each component as well as the thermal noise to the detected sample $Y_s[1]$ under an activation attempt in the scheduling period $k = 1$.

(1) Signal component: Given an activation attempt in the scheduling period $k = 1$, the signal component of $Y_s[1]$ can be written as

$$Y_s^{(s)}[1] = \int_0^T a^2|H_r(f_0)|^2\cos^2(2\pi f_0 t+\phi)\mathrm{d}t = \frac{1}{2}Ta^2|H_r(f_0)|^2. \quad (5)$$

Note that phase recovery comes for free due to the square-law device and hence our nanoreceiver avoids the associated complex circuitry for that task.

(2) Signal–noise cross-component: Given an activation attempt in scheduling period $k = 1$, the signal–noise cross-component can be written as

$$Y_s^{(\text{s-n})}[1] = \int_0^T 2a|H_r(f_0)|\cos(2\pi f_0 t+\phi)\tilde{W}_a(t)\mathrm{d}t. \quad (6)$$

Since $\tilde{W}_a(t)$ is a Gaussian process, $Y_s^{(\text{s-n})}[1]$ is a Gaussian random variable with mean $\mathbb{E}\left[Y_s^{(\text{s-n})}[1]\right] = 0$. To find the variance, we calculate

$$\begin{aligned}\mathrm{var}\left(Y_s^{(\text{s-n})}[1]\right) &= \mathbb{E}\left[\int_0^T\int_0^T 4a^2|H_r(f_0)|^2\cos(2\pi f_0 t+\phi)\right.\\ &\quad\left.\times\ \cos(2\pi f_0\tau+\phi)\tilde{W}_a(t)\tilde{W}_a(\tau)\,\mathrm{d}t\mathrm{d}\tau\right]\\ &= 4a^2|H_r(f_0)|^2\int_0^T\int_0^T\frac{1}{2}[\cos(2\pi f_0(t+\tau)+2\phi)\\ &\quad+\cos(2\pi f_0(t-\tau))]K_{\tilde{W}_a}(t-\tau)\,\mathrm{d}t\mathrm{d}\tau, \quad (7)\end{aligned}$$

where $K_{\tilde{W}_a}(\cdot)$ is the autocovariance function of the filtered noise process $\tilde{W}_a(t)$. The associated power spectral density can be written as $S_{\tilde{W}_a}(f) = \frac{N_a}{2}|H_r(f)|^2$. Here, let us define $\hat{H}_r(f)$ such that

$$|H_r(f)|^2 = |H_r(f_0)|^2\left[\hat{H}_r\left(\frac{f-f_0}{B}\right)+\hat{H}_r\left(\frac{f+f_0}{B}\right)\right], \quad (8)$$

where $B = f_0/2Q$ is the 3-dB bandwidth of $H_r(f)$. Thus, $\hat{H}_r(f)$ is the baseband representation of a sidelobe (sidelobes are symmetric) of $|H_r(f)|^2$, normalized to have a unit gain at DC frequency and a unit 3-dB bandwidth. Hence, the time-domain response of $|H_r(f)|^2$ is $2\cos(2\pi f_0 t)B\hat{h}_r(Bt)|H_r(f_0)|^2$, where $\hat{h}_r(t)$ is the inverse Fourier transform of $\hat{H}_r(f)$. Consequently, the autocovariance function of the $\tilde{W}_a$ can be written as

$$K_{\tilde{W}_a}(t) = N_aB|H_r(f_0)|^2\cos(2\pi f_0 t)\hat{h}_r(Bt). \quad (9)$$

One can realize that the variance of white noise, filtered by the antenna response, is $\sigma^2_{\tilde{W}_a} = N_aB|H_r(f_0)|^2$, where $B|H_r(f_0)|^2$ can be viewed as the "energy" of the filter response. With this, we can evaluate the variance of the signal–noise cross-component as

$$\begin{aligned}\mathrm{var}\left(Y_s^{(\text{s-n})}[1]\right) &= 2a^2N_a|H_r(f_0)|^4\\ &\quad\times\int_0^T\int_0^T\left[\cos^2(2\pi f_0(t-\tau))+\cos(2\pi f_0(t-\tau))\right.\\ &\quad\left.\times\ \cos(2\pi f_0(t+\tau))\right]B\hat{h}_r(B(t-\tau))\,\mathrm{d}t\,\mathrm{d}\tau\\ &= 2a^2N_a|H_r(f_0)|^4\left\{\int_0^T\int_0^T\frac{1}{2}[1+\cos(4\pi f_0(t-\tau))]\right.\\ &\quad\times B\hat{h}_r(B(t-\tau))\,\mathrm{d}t\,\mathrm{d}\tau+\int_0^T\int_0^T\frac{1}{2}[\cos(4\pi f_0 t)\\ &\quad\left.+\ \cos(4\pi f_0\tau)]\,B\hat{h}_r(B(t-\tau))\,\mathrm{d}t\,\mathrm{d}\tau\right\} \quad (10)\\ &\approx a^2N_a|H_r(f_0)|^4\int_0^T\int_0^T B\hat{h}_r(B(t-\tau))\,\mathrm{d}t\,\mathrm{d}\tau \quad (11)\\ &\approx Ta^2N_a|H_r(f_0)|^4, \quad (12)\end{aligned}$$

where (11) follows since the integral of the cosines are inversely proportional to f_0 and they become negligible with respect to the integral of the constant term. Also, (12) follows since $1/B \ll T$ and thus $B\hat{h}_r(B(t-\tau))$ is identical to 0 for almost all pairs of (t,τ) except for those that are very close to each other. Since the area under $\hat{h}_r(t)$ is 1, $B\hat{h}_r(B(t-\tau))$ acts as a unit impulse function $\delta(t-\tau)$.

As a result, $Y_s^{(\text{s-n})}[1] \sim \mathcal{N}(0, Ta^2N_a|H_r(f_0)|^4)$. Note that the strategy of increasing the transmit signal power, $a^2/2$, in order to reduce the time T to activate a node generally fails due to the signal–noise cross-component, since the noise level is also amplified by the signal amplitude a.

(3) Noise–noise cross-component: Regardless of whether there is an activation attempt in scheduling period $k = 1$, the noise–noise cross-component will be observed at the output of the antenna. The contribution of the noise–noise cross-component on the sample $Y_s[1]$ can be found as

$$Y_s^{(\text{n-n})}[1] = \int_0^T\tilde{W}_a^2(t)\,\mathrm{d}t. \quad (13)$$

The noise–noise cross-component has a non-zero mean: $\mathbb{E}\left[Y_s^{(\text{n-n})}[1]\right] = T\sigma^2_{\tilde{W}_a} = TN_aB|H_r(f_0)|^2$. To find the variance, we note that $\tilde{W}_a^2$ has a power spectral density with a 3-dB bandwidth identical to $2B$. Since $1/2B \ll T$, for any pair $(t,\tau) \in (0,T)^2$, $K_{\tilde{W}_a^2}(t-\tau)$ is very close to 0, unless $t \approx \tau$. Due to the large bandwidth, we write $K_{\tilde{W}_a^2}(t-\tau) \approx \sigma^2_{\tilde{W}_a^2}\delta(t-\tau)$. Consequently,

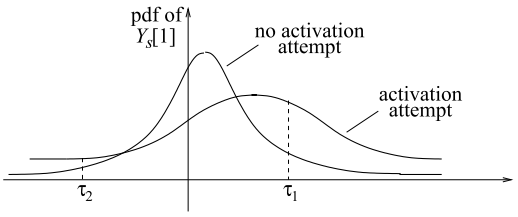

Fig. 4. The pdf of the detected signal under activation attempt and no activation attempt.

$$\begin{aligned}\operatorname{var}\left(Y_s^{(\text{n-n})}[1]\right) &= \int_0^T \int_0^T K_{\tilde{W}_a^2}(t-\tau)\,\mathrm{d}t\,\mathrm{d}\tau \\ &\approx \int_0^T \int_0^T \sigma^2_{\tilde{W}_a^2}\delta(t-\tau)\,\mathrm{d}t\,\mathrm{d}\tau \\ &= \int_0^T \int_0^T 2\sigma^2_{\tilde{W}_a}\delta(t-\tau)\,\mathrm{d}t\,\mathrm{d}\tau \qquad (14)\\ &= 2T\left(BN_a|H_r(f_0)|^2\right)^2. \qquad (15)\end{aligned}$$

One cannot disregard the noise–noise cross-component, since it can potentially be large due to the lack of a front-end filter.[3]

(4) Thermal noise: The contribution of thermal noise on the sample $Y_s[1]$ can be found as

$$Y_s^{(\text{T})}[1] = \int_0^T W_T(t)\,\mathrm{d}t. \qquad (16)$$

Clearly, $\mathbb{E}\left[Y_s^{(\text{T})}[1]\right] = 0$ and $\operatorname{var}\left(Y_s^{(\text{T})}[1]\right) = T\frac{N_T}{2}$.

With the above observations, we can write the following conditional distributions for $Y_s[1]$, using a *Gaussian approximation* for the noise–noise cross-component.
Given an activation attempt,

$$Y_s[1] \sim \mathcal{N}\left(\underbrace{T|H_r(f_0)|^2(a^2/2+N_aB)}_{\mu_p},\ \underbrace{T\left[N_a|H_r(f_0)|^4(a^2+2B^2N_a)+\frac{N_T}{2}\right]}_{\sigma_p^2}\right).$$

Given no activation attempt,

$$Y_s[1] \sim \mathcal{N}\left(\underbrace{T|H_r(f_0)|^2N_aB}_{\mu_n},\ \underbrace{T\left[2\left(BN_a|H_r(f_0)|^2\right)^2+\frac{N_T}{2}\right]}_{\sigma_n^2}\right).$$

[3] Note that the nanoantenna acts as a front-end filter to some extent. However, the bandwidth of the antenna response is fairly wide (depends on the Q factor) and it lets a significant amount of noise through.

In the subsequent analysis, we deal with the probability of two events: **unsuccessful activation attempt** and **false activation**. In the former, the activator attempts to activate a node, but the node remains inactive, whereas in the latter, the node goes active without an activation signal. We define the optimal detector [31,32] as the one that minimizes the **probability of an unsuccessful activation attempt**, p_{ua}, subject to a given **probability of false activation**, p_{fa}. Since the signal–noise cross-component is 0 without the activation signal, the total noise variance differs with and without the activation attempt as shown in Fig. 4. Thus, the optimal detector involves comparisons with multiple thresholds. Let us define $\text{SNR}_a \triangleq \frac{a^2}{2N_a}$ as the signal to acoustic noise ratio and $\text{SNR}_T \triangleq \frac{a^4}{4N_T}$ as the (power of the) observed current to thermal noise ratio. We also define p_a as the prior probability for an activation attempt in any given activation period and probability of error as the total probability of an undesirable event: $p_e = p_a p_{ua} + (1-p_a)p_{fa}$. Next, we present the detector performance in what follows.

Fig. 5 illustrates the performance of the nanoreceiver with our energy detector. To obtain these curves, we chose the parameters of the system as $f_0 = 15$ MHz, $Q = 1000$ and $p_a = 10^{-3}$. We also assumed that $\frac{1}{T} \ll B \ll f_0$, where $B = f_0/2Q$ is the 3-dB bandwidth of the antenna response $H_r(f)$.

In Fig. 5(a), we plot the probability of error as a function of the activation time T for various values of SNR_a. Here we assume that the dominant source of noise is the acoustic noise, i.e., $\text{SNR}_a \ll \text{SNR}_T$. One can find that the maximum likelihood decision rule activates the node if $Y_s[1] > \tau_1^{(\text{ML})}$ or $Y_s[1] < \tau_2^{(\text{ML})}$, where the thresholds $\tau_1^{(\text{ML})}$ and $\tau_2^{(\text{ML})}$ satisfy

$$\frac{\tau_1^{(\text{ML})}-\mu_n}{\sigma_n} = \sqrt{\frac{T}{2}}B\left(-1 + \sqrt{\left(1+\frac{\text{SNR}_a}{B}\right)\left(1+\frac{2}{T\text{SNR}_a}\log\left[\left(\frac{1}{p_a}-1\right)^2\left(1+\frac{\text{SNR}_a}{B}\right)\right]\right)}\right), \qquad (17)$$

$$\frac{\tau_2^{(\text{ML})}-\mu_n}{\sigma_n} = \sqrt{\frac{T}{2}}B\left(-1 - \sqrt{\left(1+\frac{\text{SNR}_a}{B}\right)\left(1+\frac{2}{T\text{SNR}_a}\log\left[\left(\frac{1}{p_a}-1\right)^2\left(1+\frac{\text{SNR}_a}{B}\right)\right]\right)}\right). \qquad (18)$$

Note that here we neglect $TN_T/2$ in σ_n^2, since acoustic noise is assumed to be the dominant noise source. The *minimum* error probability (p_e associated with the maximum likelihood detector) $p_e^{(\text{ML})} = p_a p_{ua}^{(\text{ML})} + (1-p_a)p_{fa}^{(\text{ML})}$, where

$$p_{ua}^{(\text{ML})} = \Phi\left(\frac{\tau_1^{(\text{ML})}-\mu_p}{\sigma_p}\right) - \Phi\left(\frac{\tau_2^{(\text{ML})}-\mu_p}{\sigma_p}\right), \qquad (19)$$

$$p_{fa}^{(\text{ML})} = \Phi\left(\frac{\tau_2^{(\text{ML})}-\mu_n}{\sigma_n}\right) + 1 - \Phi\left(\frac{\tau_1^{(\text{ML})}-\mu_n}{\sigma_n}\right). \qquad (20)$$

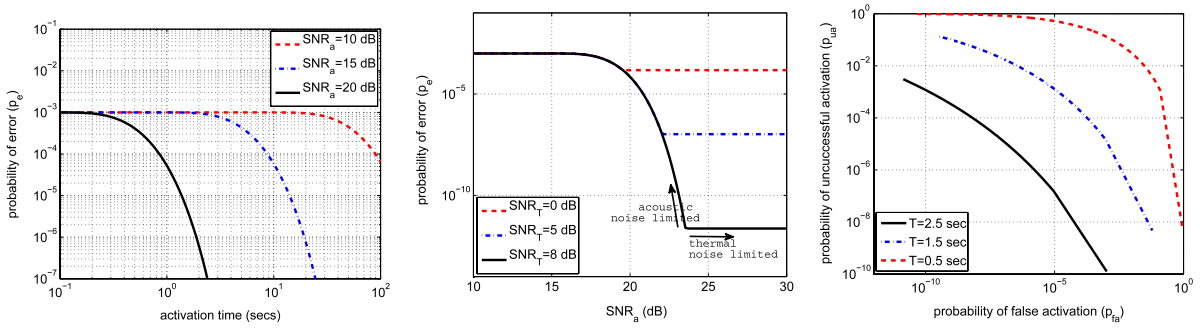

(a) p_e versus T. (b) p_e versus SNR_a. (c) p_{ua} versus p_{fa}.

Fig. 5. System performance and various tradeoffs and are illustrated for a single nanoreceiver.

One can evaluate $(\tau_i^{(\mathrm{ML})} - \mu_p)/\sigma_p$ for $i = 1, 2$ using $(\tau_i^{(\mathrm{ML})} - \mu_n)/\sigma_n$ as given in Eqs. (17) and (18) as follows:

$$\frac{\tau_i^{(\mathrm{ML})} - \mu_p}{\sigma_p} = \left(\frac{\tau_i^{(\mathrm{ML})} - \mu_n}{\sigma_n} - \sqrt{\frac{T}{2}} \frac{\mathrm{SNR}_a}{B} \right) \times \left(\sqrt{1 + \frac{\mathrm{SNR}_a}{B^2}} \right)^{-1}. \quad (21)$$

One can observe from Fig. 5(a) that, roughly with every 5 dB increment of the SNR, the activation time necessary to achieve a certain probability of error decreases by an order of magnitude. It is notable that, with $\mathrm{SNR}_a = 20$ dB, only 2 s is sufficient to achieve a $p_e < 10^{-6}$.

In Fig. 5(b), we illustrate the probability of error as a function of SNR_a for various values of SNR_T and activation time $T = 1$ s. For low values of SNR_a, the acoustic noise is the determining factor for p_e, while the thermal noise starts to dominate as SNR_a is increased beyond a certain point. One can realize that the impact of thermal noise is relatively less detrimental, compared to that of the acoustic noise. Indeed, even an SNR_T as low as 5 dB allows for $p_e = 10^{-7}$, if SNR_a is sufficiently high. The reason for the impact of acoustic noise being more severe is that, due to the lack of a front-end filter, a large portion of the cross-components cannot be filtered out by the integrator.

In Fig. 5(c), we illustrate the *receiver operating characteristics* (ROC); i.e., minimum p_{ua} achievable by our nanoreceiver for a given p_{fa} (according to the Neyman–Pearson criterion [31]) for various values of the activation time T. Here, we assume that the acoustic noise is the dominant noise source and we take $\mathrm{SNR}_a = 20$ dB. To plot these curves, we used the pair of thresholds $\tau_1^{(\mathrm{NP})}$ and $\tau_2^{(\mathrm{NP})}$, and calculated the associated values of p_{ua} and p_{fa}, based on the decision rule, "activate node if $Y_s[1] > \tau_1$ or $Y_s[1] < \tau_2$" and remain inactive otherwise. The Neyman–Pearson thresholds $\tau_1^{(\mathrm{NP})}$ and $\tau_2^{(\mathrm{NP})}$ turn out to be identical to $\tau_1^{(\mathrm{ML})}$ as in (17) and $\tau_2^{(\mathrm{ML})}$ as in (18), respectively, evaluated as the value of p_a is varied in [0, 1]. Note that this does not imply that the values of p_{ua} and p_{fa} depend on the probability of activation at all. Here, p_a is merely a parameter that gives us the Neyman–Pearson thresholds to find the minimum p_{ua} subject to a given p_{fa}. The ROC is sketched by plotting (19) versus (20) as the thresholds are varied using p_a as described above.

Fig. 5(c) illustrates the reliability of our nanoreceiver. If $T = 2.5$ s is chosen as the activation period, one can achieve a $p_{ua} = 10^{-4}$ at a $p_{fa} = 10^{-8}$. Note that, at this p_{fa} and T pair, even over a **month** of continuous operation, the probability of false activation of our node remains below 10^{-2}. Even with such a conservative selection, it is possible to achieve a probability of unsuccessful activation 10^{-4}.

We have illustrated that, even with our simple nanoreceiver, the activation of a node with very low probability of error is possible with reasonably short activation signals and at values of overall signal to noise ratio as low as 15 dB. Moreover, our nanoreceiver is reliable: it can be designed to operate over months without a false activation event and at the same time to achieve fairly low probabilities of unsuccessful activation, even with activation periods of as low as a few seconds. Lastly, the receiver performance is independent of the random phase, ϕ, of the carrier signal (due to the square-law device). Hence, our nanoreceiver avoids complex circuitry for phase recovery.

On the other hand, the performance of our nanoreceiver is highly sensitive to the Q parameter. To illustrate this, in Fig. 6(a), we plot the probability of error as a function of SNR for various values of the Q parameter of the nanoantenna for $T = 1$ s. Recall that the Q parameter is related to the 3-dB bandwidth, B, of the nanoantenna response by the equation $B = f_0/2Q$. Therefore, the higher the bandwidth, the worse the performance, since the noise power allowed is proportional to the bandwidth.

Also, frequency mismatch is an important factor that affects the system performance. In Fig. 6(b), we plot the probability of error as a function of the amount of frequency mismatch, Δf_0, normalized with respect to the resonance frequency, f_0, of the nanoantenna for various values of SNR_a at $T = 2.5$ s. Here, we take $Q = 500$, $f_0 = 15$ MHz; hence $B = 15$ kHz. One can observe that, even with a 0.1% of frequency mismatch with respect to the resonance frequency, the probability of error increases by multiple orders of magnitude. This degradation will be even more severe for nanoantennas with higher Q factors (even though the improvement is also significant). The associated *power penalty* for a 0.1% increase in the frequency mismatch can be as high as 2 dB at values of SNR_a around 20 dB.

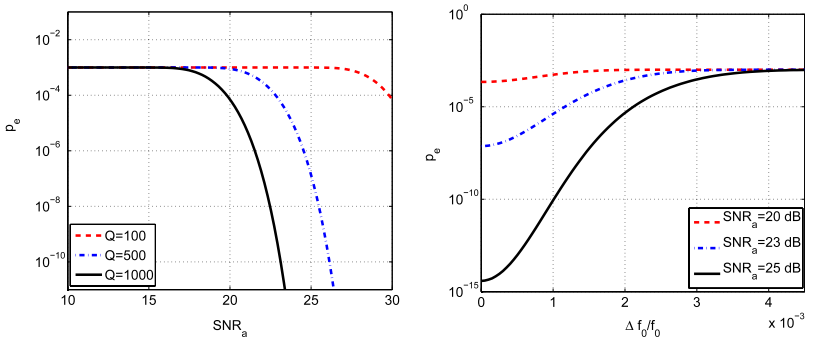

(a) p_e versus SNR_a for various Q. (b) p_e versus $\Delta f_0/f_0$.

Fig. 6. Sensitivity of system performance with respect to the Q parameter and frequency mismatch.

These results illustrate the feasibility of individual node activation in real environments using simple and realizable, and yet reliable, nanoreceivers. However, the performance is highly sensitive with respect to the nanoantenna parameters and possible imperfections due to frequency and timing mismatch.

We would like to finish this section by noting that one can achieve multiple tasks per node by waiting for multiple activation periods and interpreting sequences of pulses. Taking this idea one step further, we can actually use the nanoreceiver for **digital data communication**. Indeed, the reciprocal, $1/T$, of the activation period of the system can be viewed as the **data rate** of the communication system at the associated probability, p_e, of error. For instance, a rate of 1 bit/s is achievable at a $p_e = 10^{-6}$ at a signal to noise ratio of 20 dB. Data communication enables the possibility of more complex tasks for each node. We propose to explore nanoreceiver designs for communication of data. Important fundamental questions include whether there exists more efficient detectors than the mere energy detector and whether the required computational power to achieve the task is feasible at the nanolevel.

5. Multi-node activation

In our nanonetwork, various tasks are activated by exciting nanoreceivers at appropriate frequencies. Our basic system vision allows for a single task to be activated per nanoreceiver. Unless nodes have sufficient computational capabilities to interpret sequences of bits, the number of distinct antennas constitute a fundamental limit on the number of different tasks the nanonetwork can accommodate. In the following, we extend our analysis to a single-hop multi-receiver system.

Each antenna has a different length, and hence a different center frequency. As the number of tasks we would like to activate increases, the necessary number of antennas with different center frequencies increases. To accommodate this requirement, the channels need to be stacked closer and closer to each other. This raises the issue of **cross-channel crosstalk**. Due to the non-atomic response of the nanoantennas, antennas with center frequencies close to each other start to interfere: hence the tradeoff between the communication performance and the number of different tasks in the network. We first quantify this tradeoff.

At any given time t, consider an activation attempt at a neighboring channel, with an activation signal $Y_i'(t) = a' \cos(2\pi (f_0+\delta_c)t+\phi')$, where δ_c is the frequency spacing between neighboring channels and ϕ' is the random phase associated with the carrier of the neighboring channel. The contribution of this signal at the output of the antenna response is $Y_o'(t) = a'|H_r(f_0+\delta_c)|\cos(2\pi(f_0+\delta_c)t+\phi')$. In what follows, we treat the crosstalk as additive Gaussian noise and assume that $Y_o'(t) \sim \mathcal{N}(0, a'^2|H_r(f_0+\delta_c)|^2/2)$. Thus, the observed signal to crosstalk plus acoustic noise ratio can be written as

$$\mathrm{SCNR}_a = \frac{a^2|H_r(f_0)|^2}{a'^2|H_r(f_0+\delta_c)|^2 + N_a|H_r(f_0)|^2}.$$

To plot the following curves, we take identical carrier amplitudes, $a' = a$, and assume that all crosstalk beyond the adjacent channel is negligible. Note that we will also observe in the following analysis that this assumption is highly reasonable, since the impact of crosstalk from another channel vanishes fairly quickly beyond a certain frequency spacing.

In Fig. 7(a), we illustrate p_{ua} achievable by our nanoreceiver with $Q = 1000$, for a given p_{fa} (according to the Neyman–Pearson criterion) for various values of δ_c, at $SNR_a = 20$ dB and $T = 2.5$ s. One can observe that, while the performance remains almost unchanged for values of δ_c higher than 3 MHz, the performance degrades abruptly as δ_c decreases from 3 MHz to 1 MHz. This **phase transition** phenomenon somewhat simplifies system design. For this above set of parameters, for instance, a frequency spacing above 3 MHz is sufficient to achieve a high performance, and above this value of δ_c the performance is somewhat insensitive to the variations of δ_c. Recall that the feasible values for the lengths of nanoantennas enable us to utilize a usable bandwidth between 10 and 100 MHz. Thus, the number of tasks that the network can handle, utilizing this roughly 90 MHz of bandwidth, is ∼30 for the above set of parameters.

In Fig. 7(b), we illustrate p_e as a function of frequency spacing δ_c at $T = 1$ s, for various values of SNR_a and with the assumption that the acoustic noise is the dominant

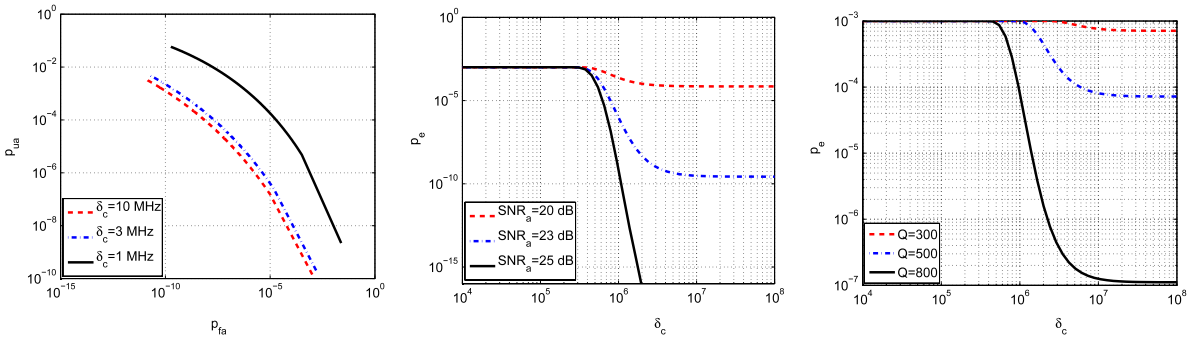

(a) p_{ua} versus p_{fa}. (b) p_e versus δ_c. (c) p_e versus δ_c for various Q.

Fig. 7. System performance and various tradeoffs and are illustrated for a multiuser nanonetwork.

noise source, $Q = 1000$ and $p_a = 10^{-3}$. Similar to the ROC plots given in Fig. 7(a), here we can also observe the phase transition phenomenon that occurs in p_e as the frequency spacing decreases. Beyond a certain point, increasing δ_c does not increase the performance significantly. That cutoff point (3–5 MHz here) is an appropriate choice for determining the number of different tasks to be activated in the nanonetwork.

Finally, in Fig. 7(c), we plot p_e as a function the frequency spacing, δ_c, of neighboring channels, for $SNR_a = 23$ dB at $T = 1$ s and $p_a = 10^{-3}$, for various values of Q and with the assumption that the acoustic noise is the dominant noise source. Similar to the single-receiver case, we observe the sensitivity of the error probability with respect to the Q parameter. This observation emphasizes the importance of antenna design to achieve a high performance.

To summarize, we observed that here is a fundamental tradeoff between the number of different tasks that a nanonetwork can execute and reliable communication over the network. Thus, one has to be careful in planning the tasks and divide the available bandwidth carefully between each node according to the task they are supposed to execute. Notably, the error performance is highly insensitive with respect to the frequency spacing, except for a phase transition at a certain point. One should be careful in order not to remain on the unfavorable side of the error curve when designing the system. However, the system performance is highly tied to the parameters of the nanoantenna; hence nanoantenna design is a critical component of network design.

6. Example application: chemical concentration control

In this section, we introduce an application of the basic communication in a system designed to control the concentration of a chemical in an environment. This example is a simple nanonetwork that can be enabled by the proposed communication paradigm. The envisioned system is composed of a nanonode that can release a predetermined amount of a chemical when activated via a nanoreceiver (Node A2 in Fig. 8), and another nanonode that measures the concentration of the chemical and emits

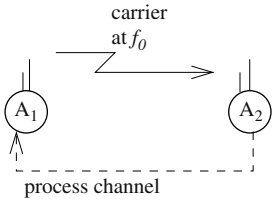

Fig. 8. Example nanonetwork architecture controlling a chemical's concentration.

an activation signal via its nanotransmitter if the measured concentration is below a particular threshold (Node A1 in Fig. 8). The information flow from A2 to A1 occurs via release and measurement of chemicals in the medium. We refer to this mode of communication as communication over the process channel. In the following, we will analyze this control system with the assumption that the only source of uncertainty is the communication channel. The process channel is assumed to work perfectly, and so do the nanonodes in their measurement and chemical release functions.

At any integer time value t, the concentration of the chemical in interest is measured to be C_t. Between each fixed activation period of length D, let the concentration decay to $\beta(D)$ of its previous value, where $0 < \beta(D) \leq 1$. The system depicted in Fig. 8 aims to maintain the concentration at a desired level, C_{des}. The system accomplishes this by releasing a fixed amount of chemicals that raises the concentration level by α. Consequently, the concentration C_t measured at time t is given by

$$C_t = \beta(D)\left[C_{t-1} + \alpha\left(a(t-1)\mathbb{1}_{P_{ca}(D)} + (1 - a(t-1))\mathbb{1}_{P_{fa}(D)}\right)\right], \quad (22)$$

where $\beta(D)$ is the rate of decay, $a(t)$ is 1 if A2 is activated to release its chemical and 0 otherwise, $P_{ca}(D)$ is the probability of correct activation, defined as $P_{ca}(D) \triangleq 1 - p_{ua}^{(ML)}$ (see Eq. (19)) and $P_{fa}(D)$ is the probability of false activation, defined as $P_{fa}(D) \triangleq p_{fa}^{(ML)}$ (see Eq. (20)), both for an activation period of D. A large D improves the probability of correct reception and reduces probability

of false activation.[4] At the same time, a large D value decreases β, which affects the control accuracy negatively. Hence, it is expected that there exist an optimal value of D. Similarly, α is another design parameter that affects the expected error term. The problem of minimizing the expected error over the operation time can be formulated as follows:

$$\min_{\alpha,D} \mathbb{E}\left[\min_{a(t-1)} \mathbb{E}\left[(C_t - C_{des})^2 \mid C_{t-1}\right]\right]. \tag{23}$$

Deferring the discussion on the minimization of the error term over D and α to a later point, we first concentrate on the minimization of expected error for a given system (i.e., fixed D and α), given C_{t-1}. In other words, we would like to minimize the expected error term over the activation actions, i.e., $\min_{a(t-1)} \mathbb{E}\left[(C_t - C_{des})^2 \mid C_{t-1}\right]$. Since D does not change at operation time, we drop this notation in the following discussion. The decision problem can be written as

$$\mathbb{E}\left[(C_t - C_{des})^2 \mid C_{t-1}, a(t-1) = 1\right] \underset{a=1}{\overset{a=0}{\lessgtr}} \mathbb{E}\left[(C_t - C_{des})^2 \mid C_{t-1}, a(t-1) = 0\right]. \tag{24}$$

Substituting Eq. (22) above, we obtain

$$\mathbb{E}\left[((C_{t-1} + \alpha \mathbb{1}_{P_{ca}})\beta - C_{des})^2 \mid C_{t-1}\right] \underset{a=1}{\overset{a=0}{\lessgtr}} \mathbb{E}\left[((C_{t-1} + \alpha \mathbb{1}_{P_{fa}})\beta - C_{des})^2 \mid C_{t-1}\right]$$

$$\beta\left[2\alpha C_{t-1}(P_{ca} - P_{fa}) + \alpha^2(P_{ca} - P_{fa})\right] \underset{a=1}{\overset{a=0}{\lessgtr}} 2C_{des}\alpha(P_{ca} - P_{fa})$$

$$(2\beta C_{t-1} + \alpha\beta - 2C_{des}) \underbrace{(P_{ca} - P_{fa})}_{>0} \underset{a=1}{\overset{a=0}{\gtrless}} 0. \tag{25}$$

In Eq. (25), any reasonably designed system that has a greater correct activation probability than false activation probability would satisfy the inequality independent of the $(P_{ca} - P_{fa})$ term. Therefore, given a measured concentration C_{t-1}, the action that minimizes the expected error is computed as follows:

$$C_{t-1} \underset{a=1}{\overset{a=0}{\gtrless}} \frac{C_{des}}{\beta} - \frac{\alpha}{2} \triangleq \eta_c, \tag{26}$$

where η_c is the threshold below which the node A2 should be activated. It is worth noting that the decision threshold is *independent* of the correct and false activation probabilities for any reasonably well-designed system, though dependence on the delay associated with activation is implicitly present through the parameter β. When $C_{t-1} > \eta_c$, the expected error term can be computed as

$$\mathbb{E}\left[(C_t - C_{des})^2 \mid C_{t-1} > \eta_c\right] = (C_{t-1}\beta - C_{des})^2 + P_{fa}\alpha\beta[(2C_{t-1} + \alpha)\beta - 2C_{des}]. \tag{27}$$

[4] Note that the $p_{ua}^{(\mathrm{ML})}$ and $p_{fa}^{(\mathrm{ML})}$ values are also functions of $\tau_i^{(\mathrm{ML})}$, $i = 1, 2$. Hence, for the same D value, multiple $(p_{ua}^{(\mathrm{ML})}, p_{fa}^{(\mathrm{ML})})$ values can be computed for different values of $\tau_i^{(\mathrm{ML})}$, $i = 1, 2$.

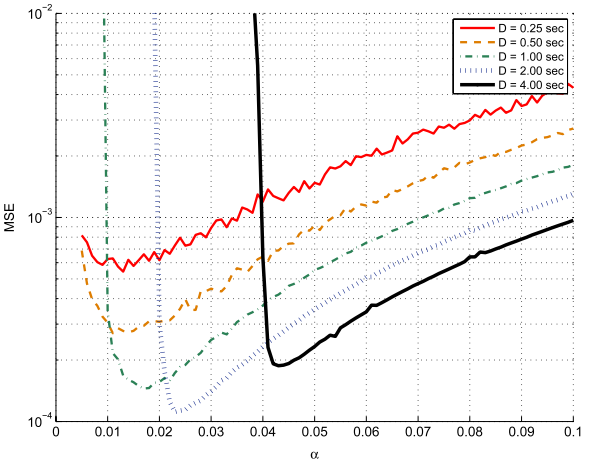

Fig. 9. Mean square error for a sample system.

Similarly, when $C_{t-1} < \eta_c$, we obtain

$$\mathbb{E}\left[(C_t - C_{des})^2 \mid C_{t-1} < \eta_c\right] = (C_{t-1}\beta - C_{des})^2 + P_{ca}\alpha\beta[(2C_{t-1} + \alpha)\beta - 2C_{des}]. \tag{28}$$

The minimization problem of Eq. (23) requires the computation of the expectation of the conditional error term $\mathbb{E}\left[\min_{a(t-1)} \mathbb{E}\left[(C_t - C_{des})^2 \mid C_{t-1}\right]\right]$, which in turn depends on the distribution of the C_t. If this expectation is known as a function of α and D, then the problem of Eq. (23) can be solved implicitly or using numerical methods, and optimal design values of α and D can be determined. Here, instead of analyzing the distribution of C_t, we provide numerical results obtained through simulations. The results depicted in Fig. 9 depict the mean square error as a function of the α parameter for four different values of D. The target concentration is selected as $C_{des} = 2$ and the concentration evolution rate as $\beta(D) = 0.995^D$. Other system-related parameters include $Q = 1000$, center frequency 90 MHz, and acoustic SNR 15 dB. For a given D value, we scan the $\tau_i^{(\mathrm{ML})}$, $i = 1, 2$, threshold values and select the pair that minimizes the MSE.

The results in Fig. 9 suggest that smaller values of α require smaller reaction times, i.e., smaller D to minimize the error. Although a small D value also reduces the correct activation probability, it is compensated by a larger β rate and rapid release of additional chemicals when needed. On the other hand, if the system is capable of delivering large quantities of chemicals in a single shot, i.e., α is large, then D must be increased, as well. A large D value means that the decay will be faster, and when the system needs to release additional chemicals, this must be done with high probability of correct activation. Also, we observe diminishing minimum MSE values as D increases from 0.25 to 2 with the appropriate selection of the α parameter. However, the minimum MSE value for $D = 4$ is greater than that for $D = 2$, which suggests that there is an optimal combination of D and α that minimizes the MSE for a given system.

7. Conclusions and future work

In this work, we have presented an analysis of a nanoscale communication systems based on carbon nanotube antennas. The system operation is based on the mechanical vibrations of the carbon nanotube when subjected to electromagnetic radiation. The mechanical response is primarily a function of the frequency of the electromagnetic waves and the length of the carbon nanotube, among other factors. The resulting communication system consists of a front end composed of the carbon nanotube antenna and an energy detector.

We explored the detection-theoretic capabilities of this simple and practical receiver, used to enable basic binary tasks that involve activation of nanodevices using pure carrier signals tuned to the resonance frequencies of the nanoantennas. We showed that, at reasonable values of SNR, our receiver is capable of being activated successfully with very high probability within a matter of few seconds and at the same time it avoids false activation even for periods of operation as long as several months. We also showed that a network of nanoreceivers can handle a large number of distinct tasks, activated simultaneously over a shared medium without a significant detriment in reliability. These analyses gave us a conceptual justification and provided design guidelines to accomplish more sophisticated tasks via interactions among multiple nanonodes equipped with carbon nanotube-based communication devices. To further illustrate this point, we presented an example application scenario where two nodes interact to control the concentration of a chemical in a given environment.

This work is the first step in developing and analyzing more sophisticated nanoscale networks. Based on the properties explored in this paper, it is possible to construct multi-hop networks consisting of nanonodes that can accomplish more complex tasks without increasing the complexity of individual nodes. To that end, the interaction between nodes and the supporting communication subsystem must be subjected to close scrutiny. The example presented in this work is only a simple example in that direction. Most importantly, a general framework that identifies key constructs of such networked systems and establishes their interactions is very much desired. Furthermore, system-wide analysis of latency, application-level accuracy and reliability are essential pieces of information to foster the design of nanonetworks. In our future work, we will explore these aspects with an emphasis on deployment scenarios and medium.

References

[1] I. Akyildiz, C.B.F. Brunetti, Nanonetworks: a new communication paradigm, Computer Networks 52 (2008) 2260–2279.
[2] O. Atakan, O. Akan, Carbon nanotune sensor networks, in: Proceedings of IEEE Nanocom 2009, 2009.
[3] J. Aylott, Optical nanosensors an enabling technology for intracellular measurements, Analyst (2003) 309–312.
[4] J. Badjic, V. Balzani, A. Credi, S. Silvi, J. Stoddar, A molecular elevator, Science 303 (2004) 1845–1849.
[5] B. Behkam, M. Sitti, Bacterial flagella-based propulsion and on/off motion control of microscale objects, Applied Physics Letters 90 (January) (2007).
[6] C. Chang, The highlights in the nano world, Proceedings of the IEEE 91 (November) (2003) 1756–1764.
[7] C. Chen, Y. Haik, J. Chatterjee, Development of nanotechnology for biomedical applications, in: Proceedings of the Emerging Information Technology Conference, August 2005.
[8] Y. Chen, G. Jung, D. Ohlberg, X. Li, D. Stewart, J. Jeppesen, Nanoscale molecular-switch crossbar circuits, Nanotechnology 14 (2003) 462–468.
[9] S. Das, C. Picconatto, G. Rose, M. Ziegler, J. Ellenbogen, System-level Design and Simulation of Nanomemories and Nanoprocessors, CRC Press, 2007.
[10] A. Das, S. Pisana, B. Chakraborty, S. Piscanec, S.K. Saha, U.V. Waghmare, K.S. Novoselov, H.R. Krishnamurthy, A.K. Geim, A.C. Ferrari, A.K. Sood, Monitoring dopants by Raman scattering in an electrochemically top-gated graphene transistor, Nature Nanotechnology 3 (2008) 210–215.
[11] E. Drexler, Nanosystems: Molecular Machinery, Manufacturing, and Computation, John Wiley and Sons Inc., 1992.
[12] A. Dubey, G. Sharma, C. Mavroidis, M.S. Tomassone, K. Nikitczuk, M.L. Yarmush, Computational studies of viral protein nano-actuators, Journal of Computational and Theoretical Nanoscience 1 (2004) 18–28.
[13] L. Foster, Nanotechnology: Science, Innovation, and Opportunity, Prentice Hall, 2005.
[14] R. Freitas, Nanotechnology, nanomedicine and nanosurgery, International Journal of Surgery 3 (November) (2005) 243246.
[15] R. Freitas, Pharmacytes: an ideal vehicle for targeted drug delivery, Journal of Nanoscience and Nanotechnology 6 (September) (2006) 27692775.
[16] R. Freitas, What is nanomedicine? Nanomedicine: Nanotechnology, Biology and Medicine 1 (November) (2004) 2–9.
[17] R Freitas, Nanomedicine, Volume I: Basic Capabilities, Bioscience, 1999.
[18] A.K. Geim, P. Kim, Carbon Wonderland, Scientific American (March) (2008) 90–97.
[19] M. Gregori, I. Akyildiz, A new nanonetwork architecture using flagellated bacteria and catalytic nanomotors, IEEE JSAC, 2010 (in press).
[20] J. Han, J. Fu, R. Schoch, Molecular sieving using nanofilters: past, present and future, Lab on a Chip 8 (January) (2008) 23–33.
[21] Intel, Technology@Intel Magazine, October, 2006.
[22] K. Jensen, J. Weldon, H. Garcia, A. Zettl, Nanotube radio, Nano Letters 7 (November) (2007) 3508–3511.
[23] A. Kiebele, G. Gruner, Carbon nanotube based battery architecture, Applied Physics Letters 91 (October) (2007) 144104.
[24] K.J. Kim, M. Shahinpoor, A novel method of manufacturing three-dimensional ionic polymer–metal composites (IPMC's) biomimetic sensors, actuators and artificial muscle, Polymer 43 (3) (2002) 797–802.
[25] J. Kong, N. Franklin, C. Zhou, M. Chapline, S. Peng, K. Cho, Miniaturized gas ionization sensors using carbon nanotubes, Science 287 (2000) 622–625.
[26] H. Lee, E. Menard, J. Tassi, G. Blanchet, Large area microcontact printing presses for plastic electronics, Materials Research Society Bulletin 846 (2005) 731–736.
[27] A. Modi, N. Koratkar, E. Lass, B. Wei, P. Ajayan, Miniaturized gas ionization sensors using carbon nanotubes, Nature 424 (July) (2003) 171–174.
[28] L. Parcerisa, I. Akyildiz, Molecular communication options for long range nanonetworks, Computer Networks 53 (November) (2009) 2753–2766.
[29] C. Peterson, Taking technology to the molecular level, IEEE Computer 33 (January) (2000) 46–53.
[30] M. Pierobon, I. Akyildiz, A physical channel model for molecular communication in nanonetworks, IEEE JSAC 2010 (in press).
[31] H.V. Poor, An Introduction to Signal Detection and Estimation, 2nd ed., Springer, New York, 1994.
[32] J.G. Proakis, Digital Communications, 3rd ed., McGraw-Hill, New York, 1995.
[33] R. Smalley, M. Dresselhaus, G. Dresselhaus, P. Avouris, Carbon Nanotubes: Synthesis, Structure, Properties and Applications, Springer, 2001.
[34] A. Tseng, K. Chen, C. Chen, K. Ma, Electron beam lithography in nanoscale fabrication: recent development, IEEE Transactions on Electronics Packaging Manufacturing 26 (April) (2003) 141–149.
[35] J. Weldon, K. Jensen, A. Zettl, Nanomechanical radio transmitter, Physica Status Solidi B 245 (October) (2008) 2323–2325.
[36] Y. Yun, C. Ah, S. Kim, W. Yun, B. Park, D. Ha, Manipulation of freestanding Au nanogears using an atomic force microscope, Nanotechnology 18 (November) (2007) 505304–505308.

C. Emre Koksal received his B.S. degree in electrical engineering from the Middle East Technical University, Ankara, Turkey, in 1996, and his S.M. and Ph.D. degrees from the Massachusetts Institute of Technology (MIT), Cambridge, in 1998 and 2002, respectively, in electrical engineering and computer science. He was a Postdoctoral Fellow in the Networks and Mobile Systems Group in the Computer Science and Artificial Intelligence Laboratory, MIT, until 2003 and a Senior Researcher jointly in the Laboratory for Computer Communications and the Laboratory for Information Theory at EPFL, Switzerland, until 2006. Since then, he has been an Assistant Professor in the Electrical and Computer Engineering Department, Ohio State University, Columbus. His general areas of interest are wireless communication, computer networks, information theory, stochastic processes, and financial economics.

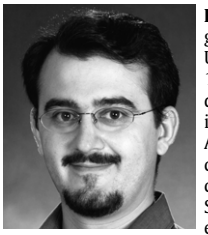

Eylem Ekici received his B.S. and M.S. degrees in computer engineering from Bogazici University, Istanbul, Turkey, in 1997 and 1998, respectively. He received his Ph.D. degree in electrical and computer engineering from Georgia Institute of Technology, Atlanta, in 2002. Currently, he is an associate professor in the Department of Electrical and Computer Engineering of The Ohio State University. His current research interests include cognitive radio networks, nanoscale networks, vehicular communication systems, and wireless sensor networks, with a focus on routing and medium access control protocols, resource management, and analysis of network architectures and protocols. He is an associate editor of Computer Networks Journal (Elsevier) and ACM Mobile Computing and Communications Review.